ChemElectroChem

Review
doi.org/10.1002/celc.202500397

Chemistry Europe
European Chemical Societies Publishing

www.chemelectrochem.org

Electrochemical Hydrodehalogenation Based on 3D-Printed Electrodes

Jennifer Christina Schmidt and Dandan Gao*

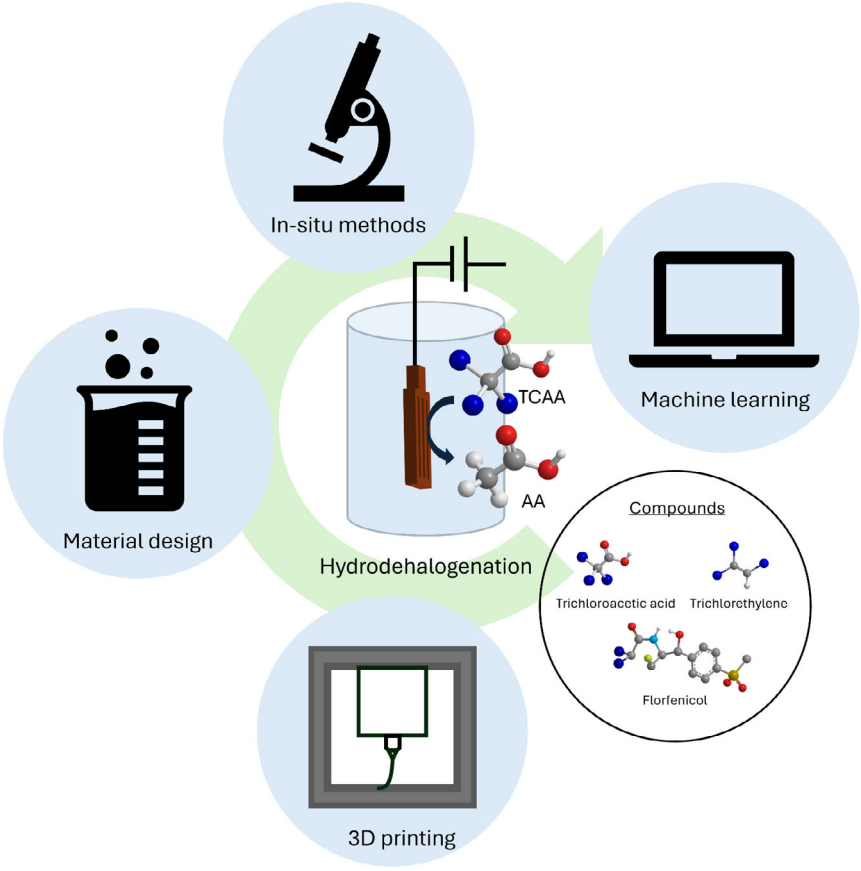

Additive manufacturing has emerged as a versatile platform for electrode fabrication, offering cost efficiency, design flexibility, and compatibility with a wide range of materials. Electrochemical dehalogenation represents a critical strategy for the removal of toxic halogenated organic pollutants, such as chloroacetic acids, which pose significant environmental and health risks. The use of earth-abundant metals, including iron, copper, and nickel, as well as carbon-based materials, further enhances the sustainability and scalability of this approach. This concept article describes the electrochemical reduction of trichloroacetic acid at conventional electrodes and reviews the current state of research on electrochemical dehalogenation at additively manufactured electrodes. From this perspective, the further integration of advanced fabrication techniques, along with the application of machine learning and artificial intelligence, presents significant opportunities for innovation in materials and processes. In addition to electrode fabrication, the incorporation of in situ spectroscopy is proposed to gain deeper insight into the underlying reaction mechanisms. To bridge the gap between fundamental research and the implementation of new processes in industrial applications, a series of process optimization strategies is also outlined.

1. Introduction

Extensive industrial usage has led to the widespread release and accumulation of halogenated organic compounds (HOCs) in the environment. Their high resistance to natural degradation processes enables them to persist for long periods and undergo long-range transport through atmospheric and groundwater pathways. The presence of halogen atoms increases the toxicity of these compounds, making them highly toxic, carcinogenic, and mutagenic to humans.[1–3] Therefore, it is necessary to develop efficient techniques to remove these pollutants. For chlorine-containing compounds, current wastewater treatment technologies include adsorption, biological methods, and chemical methods.[4,5] These methods are associated with certain limitations, including the generation of hazardous byproducts and the incomplete removal of the halogenated pollutant.[3] A more efficient and sustainable alternative is the electrochemical reduction, especially the electrochemical hydrodehalogenation (EHDH) process, which requires mostly mild reaction conditions and can be powered by renewable energy sources.[6,7] Additionally, the reaction is highly selective and does not produce toxic byproducts.[2] This approach may also be combined with a deuteration step, since halogenated intermediates constitute a suitable platform for site-specific deuterium introduction.[8,9] Concretely, the EHDH process involves the cleavage of C—Cl bonds and their subsequent replacement with C—H bonds. The reduction rate and product selectivity are strongly influenced by factors such as the choice of reducing agent and catalyst, the molecular structure of the substrate, as well as process parameters including temperature.[10] In EHDH, two principal pathways can be distinguished: in the direct pathway, electrons are transferred directly from the electrode surface to the halogenated compound, whereas in the indirect pathway, adsorbed atomic hydrogen (H*) is generated in situ and serves as the reducing agent, mediating electron transfer between the halogenated species and the catalytic sites on the electrode surface.[7] Both processes, the direct and indirect, as well as the electrode reactions, are depicted in **Figure 1**.

This review provides a comprehensive overview of electrochemical dechlorination based on 3D-printed electrodes. The following section introduces the fundamentals of EHDH, principal 3D printing techniques to establish a general understanding of the underlying technologies, followed by characterization methods of 3D-printed electrodes and a selection of recent advances in the field. The review aims to summarize the additive manufacturing methods currently employed in electrochemical applications and to highlight representative examples of 3D-printed electrodes specifically designed for dechlorination reactions. In addition, the perspective and outlook section discusses promising research directions to further enhance electrode fabrication and performance. These include the integration of machine learning (ML) tools to optimize manufacturing processes and material design, the application of in-situ spectroscopic techniques to deepen the mechanistic understanding of EHDH, and the refinement of reaction conditions through the use of pulsed potentials or flow-based systems.

2. Fundamentals and electrodes developed for EHDH

In aqueous media, selective direct reduction is hindered by the competitive hydrogen evolution reaction (HER), a limitation that can be mitigated by employing suitable catalysts to lower the overpotential for dehalogenation.[5,11] This catalyst must possess a high activity to cleave carbon–halogen bonds; Metals such as Pd, Fe, Ni, Cu, Co, and Ag fulfill these demands, since they do selectively adsorb and store H* by forming metal–hydrogen bonds.[2,6,7,11–16] Among these, Pd shows the highest activity, as it can simultaneously generate the reducing agent (H*) via the Volmer reaction and activate the C—Cl bond via adsorption at its surface.[5,17] However, its high cost, scarcity, and susceptibility

J. C. Schmidt, D. Gao
Department of Chemistry
Johannes Gutenberg University Mainz
Duesbergweg 10–14, 55128 Mainz, Germany
E-mail: dandan.gao@uni-mainz.de

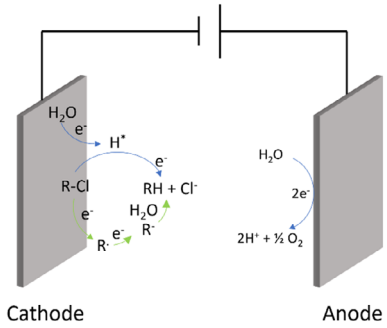

Indirect electron transfer process
$H_2O + e^- \rightarrow H^* + OH^-$
$H^+ + e^- \rightarrow H^*$
$RCl + H^+ \rightarrow RH + Cl^-$

Direct electron transfer process
$RCl + e^- \rightarrow R\cdot + Cl^-$
$R\cdot + e^- \rightarrow R^-$
$R^- + H_2O \rightarrow RH + OH^-$

Figure 1. Schematic description of the EHDH processes occurring on the cathode and anode.

to deactivation through HCl formation during the reaction limit its practical application.[18]

In contrast, earth-abundant material catalysts, including Cu, Ni, Fe, and carbon-based materials, exhibit higher activities for the direct electron transfer process.[5] Ni presents a viable alternative to Pd-based catalysts, offering lower cost and greater resistance to deactivation, while maintaining comparable activity toward hydrodechlorination (HDC).[19] Cu has been shown to be an effective catalyst, leveraging its high electrical conductivity to enhance electrocatalytic activity toward the reduction of halogenated compounds, as evidenced by the positive shift in reduction peaks. For instance, trichloroacetic acid (TCAA) can be reduced by copper at −1.3 V versus saturated calomel electrode (SCE) facilitated by strong adsorption at the electrode surface through the formation of Cu—Cl and Cu—CO bonds, highlighting the participation of the carboxylic group in this interaction.[3] Esclapez et al. demonstrated that TCAA undergoes reduction in aqueous sodium sulfate solution at potentials below -0.6 V versus Ag/AgCl, with the presence of protons and a decrease in pH enhancing the cleavage of at least the second C—Cl bond.[20] Their findings also indicated that chloroacetic acids or derivatives adsorb onto the Cu surface, as evidenced by the shift in hydrogen evolution to more negative potentials upon TCAA adsorption.

In a subsequent study, Mao et al. investigated the dechlorination of TCAA using graphene-Cu foams, revealing negligible adsorption of TCAA at the electrode surface.[2] They observed that at potentials below −1.2 V versus SCE, the reaction rate decreases due to hydrogen bubbles blocking the electrode surface. Notably, the incorporation of graphene into the Cu foam structure enhanced the removal efficiency of TCAA by nearly 100% at −1.2 V versus SCE, attributed to the graphene's layered structure, facilitating improved diffusion and electron transport. Tang et al. explored the stepwise dechlorination of trichloroethylene (TCE) at Fe–Ni/reduced graphene oxide (rGO) foams, leveraging the synergistic effects of Fe and Ni. The reducibility of Fe and low overpotential of Ni for hydrogen production were found to be crucial, with the Ni layer inhibiting Fe oxidation and enhancing hydrogen adsorption on the surface.[21]

In organic solvents, the reduction peak is usually shifted to more negative potentials than in aqueous or mixed solvents. Additionally, the catalysis via direct electron transfer is favored by more protic solvents.[22] Peters et al. didelectrolysis of lindane at Ag electrodes in different solvents, such as acetonitrile, dimethylformamide, ethanol and various mixtures. They found that, in the absence of a proton donor, chlorobenzene intermediates were formed, whereas using water as the solvent enabled complete conversion to benzene.[23]

Tang et al. highlighted the importance of pH and H* concentration in influencing the removal rates and chronoamperometric profiles of TCE dechlorination.[21] At lower pH values, a shielding effect of the protons leads to a weak electrostatic repulsion between the cathode surface and the TCE, whereas, in alkaline solution, the electrostatic repulsion is high, and therefore, the reactant can only poorly be adsorbed on the electrode surface. Additionally, at pH values < 2, the hydrogen evolution is favored, and the resulting H_2-bubbles block the surface of the electrode.[21] Since conventional electrode fabrication often relies on harsh chemical processes or external suppliers, introducing

Jennifer Christina Schmidt holds a master's degree in biomedical chemistry, during which her scientific interests in electrochemistry, materials science, and additive manufacturing were established and further developed. Her current research focuses on the development of 3D-printed electrodes for sustainable electrolysis. Through this work, she reviews modern technological approaches with the pursuit of sustainable solutions for the future.

Dandan Gao is an independent research group leader and Walter Benjamin Fellow (funded by DFG) at the department of chemistry, Johannes Gutenberg University Mainz, Germany. She received her M.S. in metal materials engineering from Shandong University, China. In 2021, she completed her Ph.D. (supervisor: Prof. Dr Carsten Streb) at Ulm University. Her current research is focused on functional material systems for sustainable chemistry, and revealing the reaction mechanisms at both atomic and molecular levels.

potential supply bottlenecks and long delivery times, an efficient and sustainable alternative is the in-house production of electrodes via additive manufacturing. In addition to material composition and reaction conditions, the geometry and surface morphology of the electrode play a decisive role in determining the electrochemical performance (EHDH).[21] In this context, additive manufacturing enables the simultaneous optimization of both material properties and structural design, facilitating the development of electrodes that provide tailored, engineered solutions and reduce dependence on scarce or toxic materials.[21]

3. 3D Printing for Electrocatalytic Applications

3.1. 3D Printing Techniques

To date, many 3D printing techniques have evolved. The Advanced Standards Transforming Market (ASTM) International suggested a classification for 3D printing methods by the type of building and bonding of the materials between the layers. The classification follows the categories: Vat photopolymerization (VP), powder bed fusion (PBF), material jetting (MJ), binder jetting (BJ), material extrusion (ME), sheet lamination (SL), and direct energy deposition (DED).[23] A more detailed overview is described in the following (**Table 1**):

The main principle of every technique is building material (e.g., metal, polymers, gels) layer-by-layer. The model is usually built in a 3D modeling computer-aided design (CAD) software and converted into a standard triangle language (STL) or 3D manufacturing format (3MF) file, which are common data transfer formats in additive manufacturing. Afterward, these files are processed in a slicing software, which turns the 3D information into the 2D layer information the printer software can use (**Figure 2**).[25]

In the following, the method of ME and PBF will be explained in more detail, since these are the most common ones used in electrocatalytic applications.

In ME processes, a polymer-based material is forced through a nozzle and deposited layer-by-layer on a surface. The material can be polymeric filament, thermoplastic polymer, pastes/gels, or dispersions. The working principle is schematically shown in **Figure 3**. Solidification occurs by cooling heated material, a curing agent triggering a chemical reaction in the material, leading to a strong bridging of the polymer molecules, residual solvents, or drying of wet materials. The most common techniques are fused deposition modeling (FDM) and direct ink writing (DIW). FDM printing a polymer filament is liquified by a heater inside the printer head a fed through a heated nozzle. Solidification happens by cooling. The advantages of this method are the wide availability of printing equipment as well as easy handling. Disadvantages are layer thickness, low resolution, and the need for support structures. These points limit the degree of complexity which can be reached with FDM.[26] The most common materials are polylactic acid (PLA), polyethylene terephthalate glycol (PETG), and acrylonitrile-butadiene-styrene (ABS) since their manufacturing properties make them easy to handle, but also more complex materials are available, e.g., polyetheretherketon, polypropylene (PP), nylon, and thermoplastic polyurethanes (TPU).[27] Composite materials are available, where the base is still polymeric material, but functional fillers such as metal powders, carbon substrates, glass, or wood are incorporated. Metal FDM printing is a compromise between the industrial-applicable SLM printing and the cost-effective and accessible FDM printing.[28] This broad material selection makes FDM printing available

Table 1. Summary of the current additive manufacturing techniques with description of the working principle, examples, materials and literature sources.

Additive manufacturing process	Working principle	Examples	Materials	Sources
Vat photopolymerization	Liquid photopolymers are deposited into a light-curing vessel (vat)	Stereolithography, digital light processing	Polymers, ceramics	[24,86,87]
Powder bed fusion	Thermal energy melts powder material together	Selective laser sintering/melting, electron beam melting, direct metal laser	Polymers, ceramics, metals, composites	[88–92]
Material jetting	Material is deposited as droplets	PolyJet, multi-Jet, 3D plotting	Polymers, ceramics, metals, composites, biological gels	[93–95]
Binder jetting	Liquid binding agent fuzes powdered material together	3D printing	Polymers, ceramics, metals, composites	[95–98]
Material extrusion	Material is liquefied and extruded through a nozzle	Fuzed deposition modeling, fuzed filament fabrication, direct ink writing/robocasting	Polymers, composite materials	[30,31,33,79,99–103]
Sheet lamination	Material is bound together in the form of sheets	Laminated object manufacturing, ultrasound consolidation	(No specific materials listed)	[104]
Direct energy deposition	Thermal energy melts material together	Direct metal deposition, electron beam additive manufacturing	Metals, hybrid materials	[105]

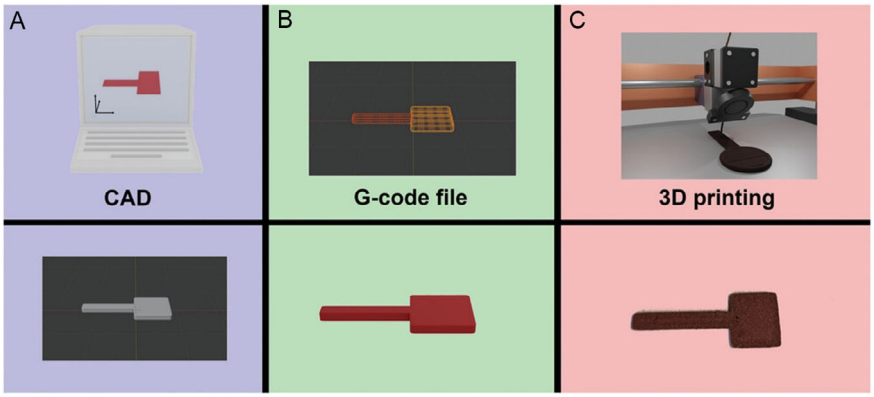

Figure 2. Schematic description of the 3D printing process. A) CAD, B) G-code file, and C) 3D printing. Reproduced with Permission.[25] Copyright 2023, Wiley-VCH.

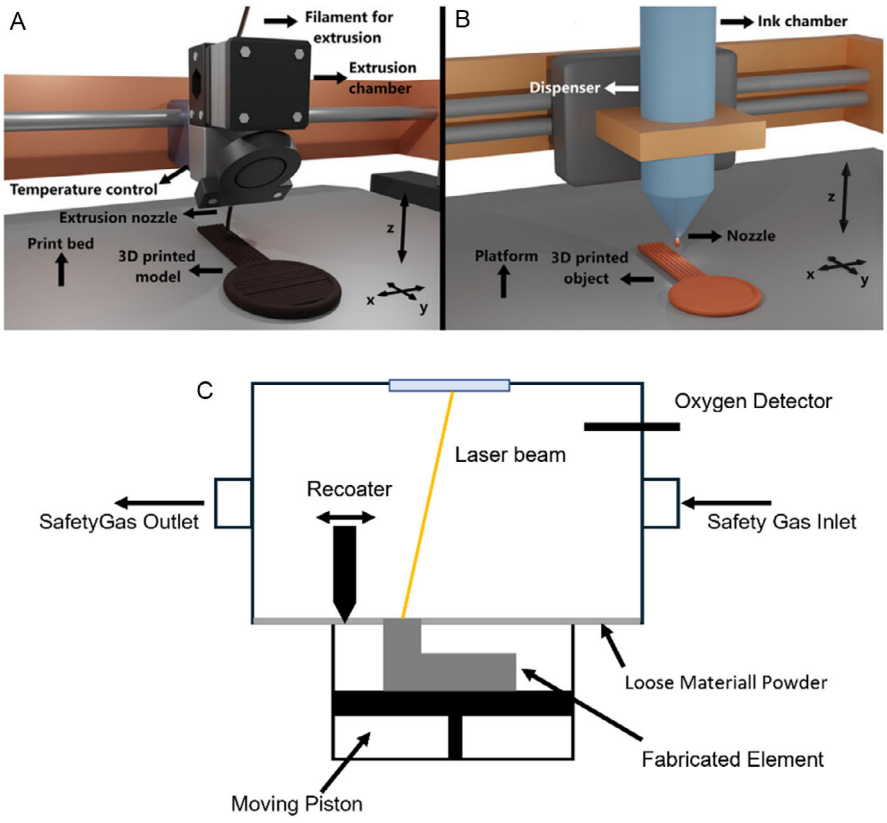

Figure 3. Schematic explanation of extrusion-based printing techniques. A) FDM and B) DIW. Reproduced with Permission.[25] Copyright 2023, Wiley-VCH. C) The general working principle of the SLM, SLS, and EBM printing techniques.

for different industries and their special needs regarding specific material properties. However, the quality of the printed part is highlydependent on the printing parameters, which are mainly the layer thickness, infill pattern, infill density, raster angle, raster width, printing speed, build orientation, nozzle, and bed temperature.

However, the parts still lack mechanical and anisotropic properties.[29] Many researchers have conducted studies on optimizing the quality of the printed parts by focusing on different process parameters.[30–32] DIW is another extrusion-based technique in which viscoelastic ink is pressed through a nozzle and deposited layer-by-layer. The solidification occurs either via cooling or with curing agents. It can be used with various materials, such as polymers, ceramics, graphene, and metals.[33] This technique is therefore mainly limited by the rheological behavior of the ink than the material class and offers the possibility of 4D printing, meaning

changing one function in dependence on an external stimulus.[34,35] Properties such as conductivity can be implemented by mixing in graphene powder or carbon nanotubes.[35,36]

PBF processes represent a widely employed category of additive manufacturing techniques with significant relevance for electrocatalytic applications. In these processes, energy provided by either a laser or an electron beam is transferred into the powder bed, where it is converted into thermal energy to induce particle bonding. After the consolidation of each layer, the build platform is lowered by one layer thickness, while the surrounding powder bed serves as a natural support medium.[27] The techniques within this category are selective laser melting (SLM), selective laser sintering (SLS), and electron beam melting (EBM).

In SLM, which is predominantly applied for metallic systems, the powder particles are fully melted and subsequently resolidified upon cooling.[27] To mitigate oxidation of the heated particles, the process is conducted in an inert gas atmosphere. In addition, preheating of the powder bed can be employed depending on the feedstock Material to reduce solidification defects and minimize cooling rates. The resulting components typically exhibit high mechanical strength as well as enhanced corrosion resistance.[37] The method offers considerable versatility, as it is compatible with a broad spectrum of materials, including Fe, Ti, Al, Ni, Co, and Cu-based alloys, as well as composite systems.[36–41] A key advantage of SLM is the ability to tailor the microstructure and, consequently, the material properties of the printed parts by adjusting the processing parameters, thereby enabling a wide range of tunable characteristics.[37]

In contrast, SLS does not involve complete melting; instead, the powder particles are sintered together. This technique can be applied to both metals and polymers.[27] EBM utilizes an electron beam to melt metallic powders within a high-vacuum chamber at elevated temperatures ($>$870 K).[28] Compared to SLM, the process involves a larger number of parameters and is restricted to a narrower range of feedstock materials.[37] Although the fundamental differences between these PBF methods may appear subtle, they exert a decisive influence on both the potential fields of application and the structural properties of the manufactured components.

3.2. Characterization of 3D-Printed Electrodes

3D-printed electrodes offer many advantages over conventionally manufactured electrodes, such as customization, uniform, and sustainable production, as well as stable and more efficient performance.[43,44] They are usually characterized by several surface characterization methods, for example scanning electron microscopy (SEM) and energy-dispersive spectrometry (EDS) for morphology and composition. X-ray diffraction (XRD), X-ray photoelectron spectroscopy (XPS), and Raman spectroscopy are used for analyzing the crystalline structure and composition of the electrode.[44–46] Additionally, the surface roughness can be analyzed by using optical microscopy or a surface roughness tester.[47] Atomic force microscopy (AFM)[48] can also be used to determine the morphology of 3D-printed parts. Other properties that can be used for the characterization or comparison of electrodes are wettability, electrochemically active surface area, and charge–transfer resistance.[49]

Neukäufer et al. investigated the results of the surface morphology of both 3D-printed specimen and conventionally produced samples via AFM and contact angle measurements. The surface roughness of the 3D-printed samples was higher compared to the conventionally produced samples, and therefore, the contact angle of the tested conventional parts was higher than of the 3D-printed parts.[48] The performance of 3D-printed electrodes can be compared to conventionally produced electrodes as well to show their superior electrocatalytic behavior. For instance, Xu et al. compared their 3D MoS_2/Nickel electrodes to hydrothermally produced electrodes, where molybdenum sulfide is deposited onto a Ni sheet.[43] They focused on the removal efficiency toward florfenicol (FLO), the degradation kinetic, and reusability and stability of the different electrodes. The 3D-printed electrodes had a higher stability during electrolysis and a lower overpotential than the hydrothermally manufactured electrode. Liu et al. compared the degradation kinetics and efficiencies of a 3D-printed MoS_2-stainless steel electrode to MoS_2-stainless steel powder for peroxymonosulfate activation.[46] They found that the processing of the material via 3D printing promotes more active sites and the kinetics were increased as well, leading to a higher degradation activity.[46]

Apart from the material aspect, geometric flexibility is an important aspect in 3D printing since structure can have impact on surface area, nucleation sites, or flow improvement. Cracks and geometric features forming edges, as well as the surface wettability, can influence the bubble formation and detachment, as shown in **Figure 4**A,B. Kou et al. compared the effects on bubble removal in alkaline water splitting of a commercial nickel foam and a 3D-printed Ni lattice structure. They found that the 3D-printed structure could prevent bubble trapping through an ordered structure and enhance uniform flow through the electrode.[50] Iwata et al. researched the effect of porous surface structure and wettability on the performance in alkaline water splitting and claimed that the controlled porosity is vital for decreasing the overpotentials due to bubble nucleation. This porosity and surface structuring can be done while printing, so no postprocessing steps are necessary for the electrodes.[51] Lee et al. designed electrodes with small cones on the surface to increase the surface area (Figure 4C,D).[52] Yang et al. investigated the effect of pore size and surface area for the improvement of the alkaline water splitting reaction.[53]

Engineering highly porous structures with a large surface area can enhance the distribution of the electrodes flowing, causing less local current density accumulation. Additionally, the electrolyte flow is enhanced and therefore the kinetics. Therefore, high surface-to-volume ratios can help to further distribute and use active materials as well as distribute the electrolyte penetration along the electrode. This is most important for high performance as well as very difficult applications.[54] One example is given by Limper et al., where they describe the manufacturing of a composite porosity mixer electrode made by SLM (**Figure 5**A). The

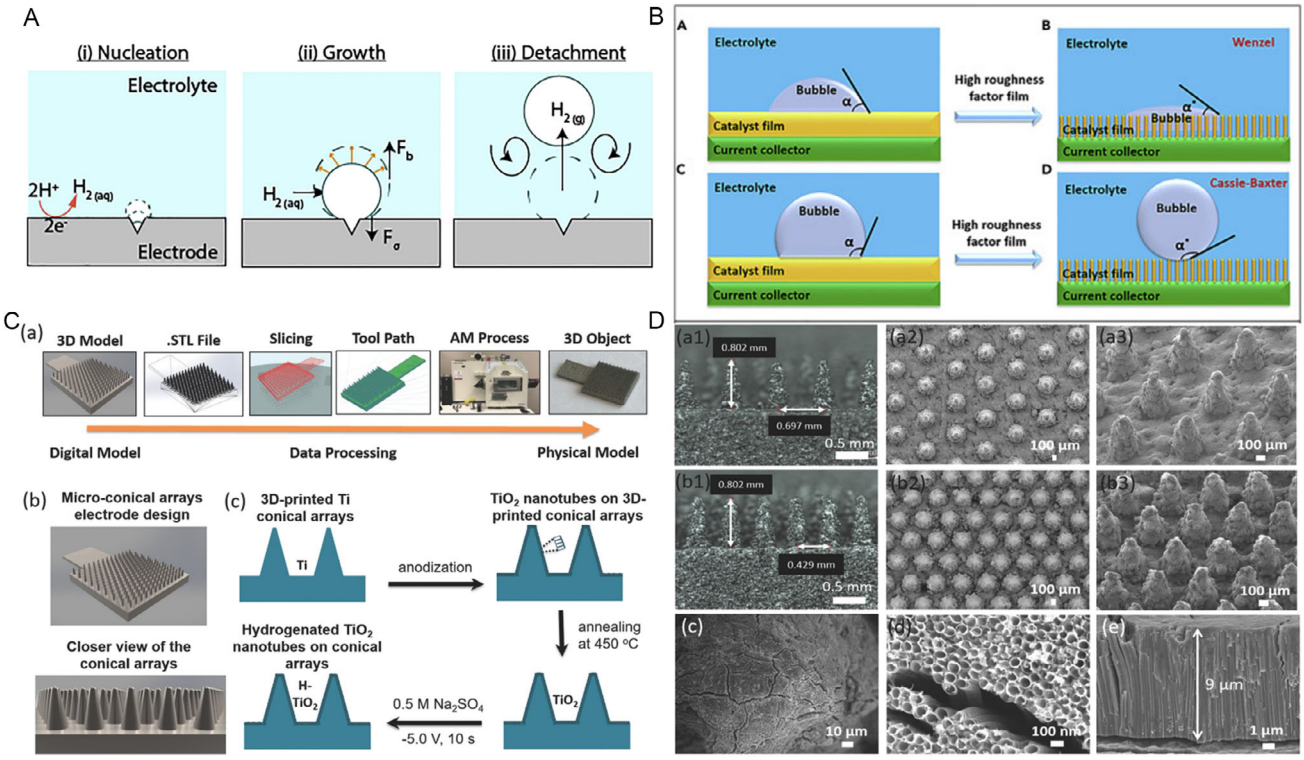

Figure 4. A,B) Schematic drawing on the formation of bubbles on electrode surfaces.Reproduced with Permission,[84,85] Copyright 2018 and 2020, American Chemical Society and Elsevier). C,D) Images of fabricated conical structures on the electrodes surface. Reproduced with Permission.[52] Copyright 2017, Wiley-VCH

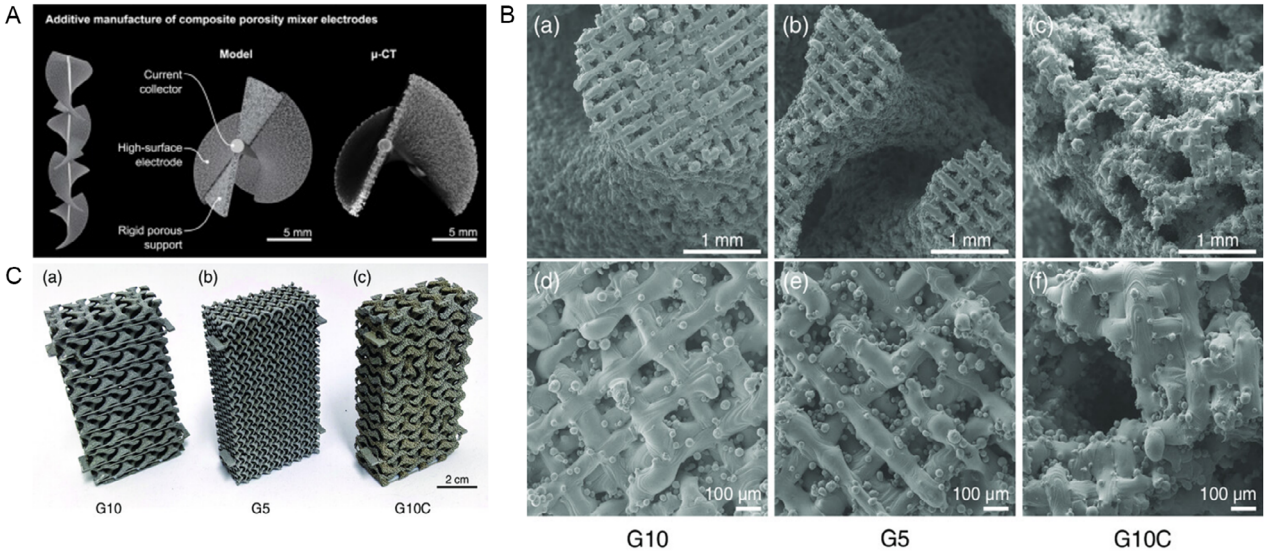

Figure 5. A) Images of SLM manufactured porous mixer structures made from stainless steel powderReproduced with Permission.[56] Copyright 2022, Elsevier. B) SEM images of intertwined gyroid structure electrodes and C) Image of gyroid structure electrodes in different sizes by Wiesner et al.[56] Reproduced with permission.[56] Copyright 2023, Elsevier.

advantages of this geometry are enhanced electrolyte mixing, and therefore eliminating mass transport limitations. They state that this structure can not only be produced by additive manufacturing, but this approach gives more variety for further design varieties, which can be implemented in one production step.[55] In addition, Wiesner et al. presented an intertwined electrode setup with a gyroid structure, which can enhance mass transport and limit diffusion boundaries at the surface (Figure 5B,C).[56]

3.3. Current Applications in EDCH

3D printing has evolved into a technology that not only can be used in mechanical applications but is also more used in other fields like medicine and biomedical research, sensing devices, for automotive and aerospace industry, and robotics.[37–40] In chemical research, especially in electrochemistry, most of it is focused onelectrodes, reactors, or flow devices for electrocatalytic reactions or electroanalytic sensing applications.[41,42] The target reactions are most commonly hydrogen evolution, nitrate reduction, and CO_2 reduction.[49,57] Some groups have started employing 3D printing to address more special reactions such as dehalogenation reactions.[42,43,45]

Zhang et al. developed a Nb_2O_5/Ti electrode via SLM 3D printing, which was used for the defluorination of FLO.[43] The Nb_2O_5/Ti electrode was used as anode, and electrochemical testing was performed in a single-chamber reactor with a solution of 5 mg/L of FLO and 30 mM of Na_2SO_4 as supporting electrolyte. Titanium powder was blended with varying weight percentages of Nb_2O_5 powder by ball milling. The resulting mixture was subsequently dried, sieved, and processed into electrodes using SLM. The additive manufacturing process produces electrodes with an open and porous architecture, which facilitates improved mass transport and efficient removal of gas bubbles.[43] The electrochemical performance of the fabricated electrodes was evaluated in different reactant systems and compared to that of an unmodified titanium electrode.[43] The addition of Nb_2O_5 powder enhanced the specific surface area and therefore increased the quantity of active sites. Additionally, it is known that an increased amount of Nb_2O_5 reduces the grain size of TiO_2 nanoparticles due to an enhanced stability against coursing. Therefore, the denser anatase phase of TiO_2 is produced at the electrode surface in the presence of Nb_2O_5, which was measured in XPS experiments.

Via SEM and EDS mapping experiments, which are shown in **Figure 6**A–F, it could be shown that an evenly distributed surface composition of the metals could be retained by SLM. The effect of Nb loading was further investigated as various Nb_2O_5 powder contents (0, 0.5, 1, 3 and 5 wt%) were tested. It was found that

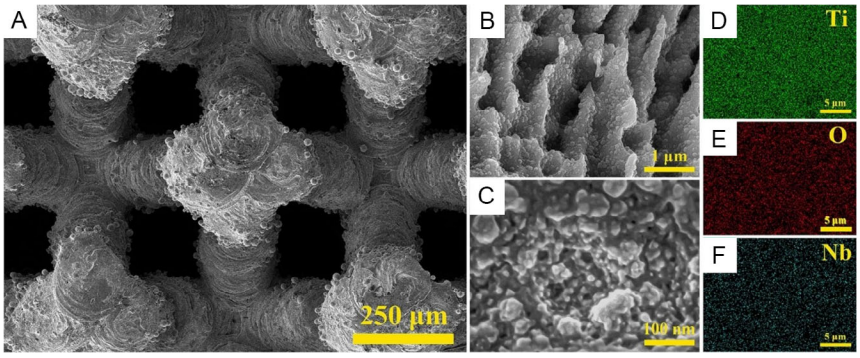

Figure 6. SEM images of the 3DP 3% Nb_2O_5/Ti electrode at magnifications of A) 250 µm, B) 1 µm, and C) 100 nm; corresponding EDS elemental maps of Ti, O, and Nb for the 3DP 3% Nb_2O_5/Ti electrode are shown in D–F). Reproduced with Permission.[43] Copyright 2023, Elsevier.

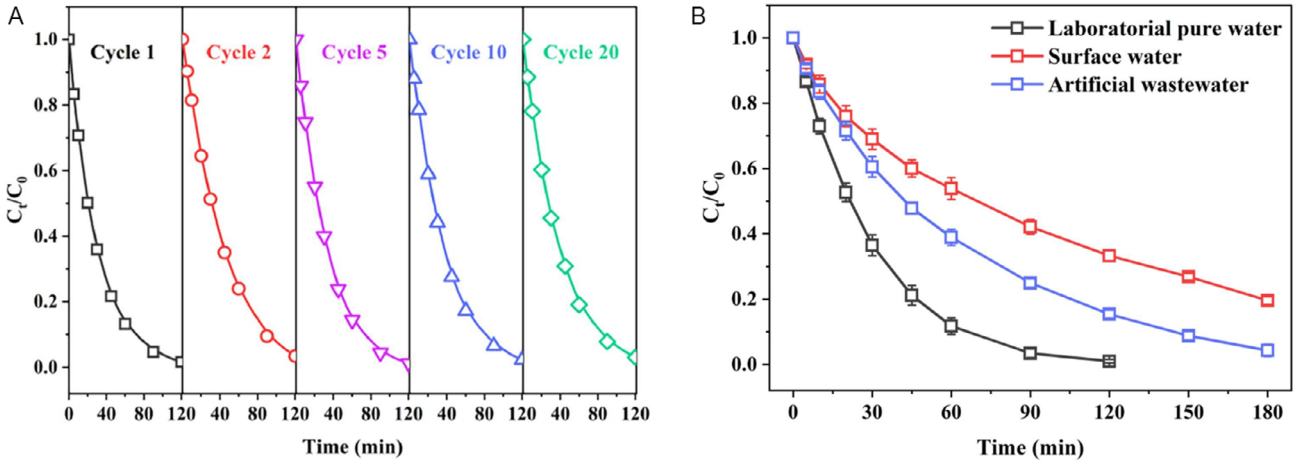

Figure 7. A) Recycling performance of the 3DP 3% Nb_2O_5/Ti electrode for the electrochemical degradation of FLO (conditions: 5 mg L^{-1} FLO, 30 mM Na_2SO_4, applied current density 20 mA cm^{-2}, initial pH 7.0). B) Application of the 3DP 3% Nb_2O_5/Ti electrode for the removal of FLO from laboratory-pure water, artificial wastewater, and surface water. Reproduced with Permission.[43] Copyright 2023, Elsevier.

the degradation efficiency for FLO increased by increasing the Nb_2O_5 content, but decreased when adding 5 wt% of Nb to the Ti powder. Assumably, the electrochemical surface area decreases by an excess of Nb powder. In electrochemical experiments, Zhang et al. calculated the oxygen exchange potential (OEP): higher OEP means that the capacity of the electrode to accumulate hydroxyl radicals is higher and therefore the generation of ROS is enhanced, which leads to a higher oxidation ability in aqueous solutions. This was also concluded as a reason why the degradation of FLO happens faster at the Nb_2O_5/Ti electrode. Moreover, the surface of the electrode serves as a trapping site for electrons from either H_2O or FLO. This is concluded to be connected to the ionic structure of the electrode surface. Since the ionic radius of Nb^{5+} (0.64 A) is comparable to Ti^{4+} (0.605 A), it is assumed that the Nb^{5+} can intercalate much easier into the Ti^{4+} lattice during the SLM process. Increasing the Nb content to 5 wt% resulted in a decrease of the measured parameters, which lays supposably in a substitution limit for the Nb^{5+} ions into the Ti lattice. Therefore, it is possible to use the Nb^{5+} as dopants than a substitution of Ti^{4+}.

The electrode's cyclability, shown in **Figure 7**, depends on reaction conditions. In acidic solutions (pH < 3), hydrogen generation competes for electrons and forms bubbles, reducing hydroxyl radicals and slowing FLO degradation. Tests in laboratorial pure water, contaminated surface water, and prepared wastewater showed the highest removal in laboratorial water and the lowest in surface water, likely due to competing species.[43]

Xu et al. developed MoS_2/Ni electrodes via SLM to enhance the dechlorination of FLO, leveraging the performance of Ni in

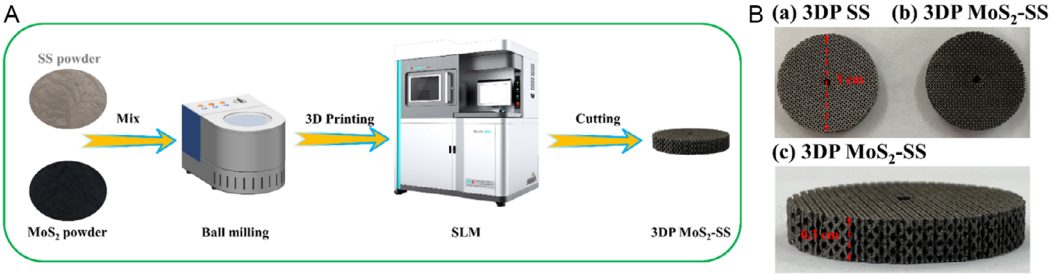

Figure 8. Production process of the electrodes. A) 3D-printed stainless steel, B) 3D-printed MoS_2-stainless steel and side view of MoS_2-stainless steel. Reproduced with Permission.[45] Copyright 2024, Elsevier.

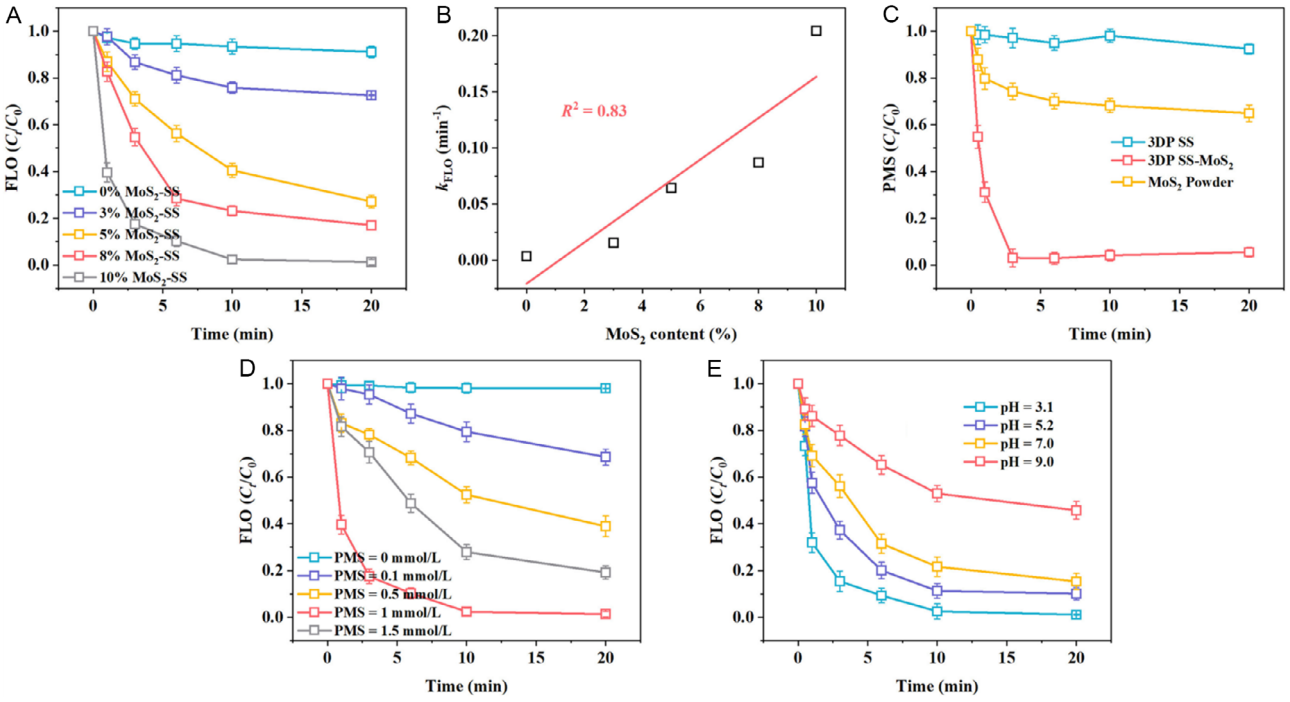

Figure 9. A) Effect of MoS_2 content in 3DP MoS_2-SS on FLO degradation. B) Variation of k_FLO with different MoS_2 contents. C) PMS decomposition performance in 3DP SS/PMS, MoS_2/PMS, and 3DP MoS_2-SS/PMS systems. Influencing factors for FLO degradation by 3DP MoS_2-SS: D) PMS dosage and E) initial pH. Experimental conditions: 10 mg L^{-1} FLO, 1 mmol L^{-1} PMS. Reproduce dwith Permission.[45] Copyright 2024, Elsevier.

dehalogenation reactions while boosting its reductive ability with MoS_2.[42] The incorporation of MoS_2, known for its excellent catalytic properties in the HER, aimed to improve the electroreductive activity of the Ni electrodes. It was found that the 3D-printed MoS_2/Ni electrode with 8% MoS_2 outperformed other compositions, achieving the highest removal efficiency after 120 min. Notably, this optimal composition also bridged the performance gap with the hydrothermally developed MoS_2/Ni electrode, which initially exhibited a higher first-order kinetic but eventually matched the efficiancy of the 3D-printed electrode. Producing these electrodes via additive manufacturing solves the issue of poor distribution of the MoS_2 and time-consuming postprocessing.[42] Durability tests further highlighted the superiority of the 3D-printed MoS_2/Ni electrode, which maintained its stability over 50 cycles with minimal overpotential in alkaline conditions, whereas the hydrothermal MoS_2/Ni electrode degraded significantly after just five cycles due to Mo leaching. This study underscores the potential of integrating MoS_2 into Ni electrodes via SLM to enhance dechlorination efficiency and durability, attributed to the increased electrochemically active surface area and facilitated interfacial electron transfer rate.

Liu et al. developed a MoS_2-stainless steel (MoS_2-SS) system for the activation of peroxymonosulfates for the dechlorination of FLO. Therefore, the electrodes with different mass ratios of MoS_2 were produced via SLM (**Figure 8**A) and compared to the 3D-printed substrates with the powder catalyst as well as a 3D-printed stainless steel substrate (Figure 8A).

The electrochemical tests were conducted in a single-chamber cell. Both the powder as well as the printed substrate could degrade FLO properly, but more active sites could be utilized by the 3D-printed substrate. The highest removal rate of FLO could be reached by a mass ratio of 10% MoS_2 and a pH value of 3.1, as shown in **Figure 9**A,E.[45]

4. Conclusion and Outlook

Electrocatalysis is increasingly recognized as a central field with the potential to advance environmentally sustainable strategies in green chemistry. A critical aspect in this regard is the use of earth-abundant and cost-effective materials, which can significantly reduce reliance on scarce and expensive resources. Numerous approaches have already been explored to improve their intrinsic performance.[48] At the same time, emerging technologies such as artificial intelligence (AI)[59,60] and additive manufacturing (e.g., 3D printing)[61,62] are opening new opportunities to accelerate the discovery and development of high-performance materials. These tools not only make research more efficient but also enable considerable savings in time and resources.[63] Addressing global environmental challenges such as pollution will require collaborative and interdisciplinary research efforts that bring together expertise across different scientific fields, highlighting the urgency of innovative and collective approaches.

4.1. AI in Electrochemical Application and Material Development

In this context, the integration of AI with additive manufacturing represents a particularly promising development, with the potential to reshape both production and materials discovery. Automated defect detection and correction, together with data-driven material development, are emerging as powerful tools. For instance, Brion et al. demonstrated a camera-based method capable of identifying and correcting errors during extrusion processes while also exploring new materials through parameter scans.[64] In SLM processes, many in situ monitoring techniques can be used for defect detection. The aim of in situ monitoring is to collect data while fabricating to get real-time quality feedback from the print.[65] Beyond manufacturing applications, AI-supported material design has also become an increasingly important driver in the development of electrocatalysts and can also be done by additive manufacturing as discussed earlier.[42] By integrating computational and experimental approaches, researchers can now predict the composition and structure of catalysts with greater accuracy, enabling rapid screening and accelerating the identification of promising candidates.[66] Moreover, ML-guided strategies provide powerful tools for both optimizing catalytic performance and enhancing durability.[67] For example, ML models can uncover correlations between 3D electrode structure and degradation pathways, thereby enabling the prediction and rational design of robust catalyst architectures via advanced 3D printing techniques. By guiding catalyst manipulation, these approaches substantially reduce experimental workload and time investment.[67]

4.2. In Situ Spectro-Electrochemistry

To gain a deeper understanding of the reaction mechanisms governing electrocatalysis, in situ characterization techniques represent indispensable tools.[68] These methods enable the correlation of the catalyst's physical and chemical structures with its activity and the associated reaction pathways.[69,70] For example, fourier transform infrared (FTIR)[71] and Raman spectroscopy[72] offer structural insights into surface-formed species and adsorbates, and can be complemented by differential electrochemical mass spectrometry (DEMS).[73] Transmission electron microscopy (TEM)[74] enables visualization of dynamic structural and morphological evolution at the nano- to atomic scale, while X-ray absorption spectroscopy (XAS)[75] captures transformations in the local chemical environment of the probed element, providing precise information on electronic structure, bond lengths, oxidation states, and coordination environments under operating conditions. In addition, XRD[76] allows tracking of crystal structures and phase transitions, and X-ray photoelectron spectroscopy (XPS)[77] provides information on surface elemental composition and oxidation-state changes during operation. Applying these approaches to dehalogenation reactions may facilitate a more comprehensive understanding of the processes occurring at the electrode–electrolyte interface, thereby linking material

properties to catalytic performance. Such insights could ultimately guide the rational design of more efficient electrode materials and the optimization of reaction parameters.

4.3. Recycling of Spent Electrode Materials

In the context of electrode materials, research efforts are not only directed toward the development of novel and more efficient compositions but also toward the recycling and reuse of spent materials to promote a more sustainable utilization of natural resources. Chodankar et al. demonstrated the potential of such an approach by recovering carbon materials from used supercapacitors and subjecting them to thermal treatment to restore their surface characteristics and structural integrity. The regenerated carbon material was subsequently re-employed in supercapacitor assemblies, exhibiting favorable electrochemical performance. These findings highlight that recycling strategies can contribute to the realization of sustainable and stable electrochemical devices.[78] To date, most research on material recycling has focused on spent lithium-ion batteries and other energy storage devices, whereas comparatively little attention has been given to the recovery and reuse of electrodes employed in electrocatalytic applications. In this regard, the recycling of materials used for 3D-printed electrodes, both polymer-based and metallic, presents an intriguing opportunity. For instance, polymer-based electrodes fabricated via FDM could be collected, shredded into granules, and re-extruded to produce new filament spools for electrode fabrication. However, further investigation is required concerning the functional filler materials, such as carbon or graphite powders, to ensure the preservation of their electrochemical activity. It is also well established that the mechanical properties of polymers can degrade over successive extrusion cycles.[79] Consequently, a detailed assessment of material property changes is essential, particularly given their strong influence on printability and structural integrity. Moreover, variations in the composition or distribution of additives may hinder effective recycling, as uneven dispersion or compositional shifts could adversely affect both the extrusion and printing process as well as the performance of the resulting electrodes.[80]

4.4. Optimization of Processes and Implementation on an Industrial Scale

In addition to the material-dependent properties discussed throughout this work, process optimization also plays a crucial role in enhancing the efficiency of the dichlorination reaction. As previously noted, in situ spectroelectrochemical techniques can be employed to elucidate the underlying reaction mechanism. Once the mechanistic pathways are well understood, such insights can be translated into practical strategies for performance improvement. For instance, the application of pulsed or potential-cycling techniques may increase reaction efficiency, such as the sequential reduction of TCAA to dichloroacetic acid, monochloroacetic acid, and acetic acid may occur at distinct potentials. Consequently, alternating between two or more potentials could enhance removal efficiency without the need to modify the electrode material or electrolyte composition. Moreover, introducing electrolyte flow could further improve the reaction performance by mitigating mass transport limitations and stabilizing local pH variations through continuous replenishment of the electrolyte solution. Increased reaction rates lead to larger diffusion layers on the surface of the electrodes, hindering the reaction.[54,81] Some work has already been done by integrating not only flow but also controlling the mass transport inside an electrochemical reactor by introducing turbulence-promoting structures or static mixers, which can also act as electrodes.[55,82,83]

In conclusion, this article provides a comprehensive overview of the current state of research on 3D-printed electrodes for electrochemical dehalogenation reactions. Given the widespread occurrence of HOCs and the critical need for their efficient removal, innovative technologies offer substantial potential to enhance existing remediation strategies. The EHDH of TCAA is presented as a representative case study, alongside various electrode materials that prioritize the use of earth-abundant and sustainable elements. Additionally, the application of 3D-printed electrodes for the dehalogenation of the veterinary antibiotic FLO has been explored, with several approaches reported in the literature, demonstrating both the feasibility of this strategy and its potential for broader applications. Looking ahead, the integration of ML techniques could further advance this field, particularly in areas such as print monitoring, material development, geometric optimization, and process parameter tuning. Beyond the optimization of individual components, a deeper mechanistic understanding achieved through in situ spectroscopic and electrochemical characterization will be crucial for improving performance. Finally, pioneering efforts toward the translation of these methods into industrial applications represent an essential future direction for this research area.

Acknowledgements

Johannes Gutenberg University Mainz is gratefully acknowledged for financial support. D.G. acknowledges the Deutsche Forschungsgemeinschaft (DFG) for a Walter Benjamin Fellowship (project no. 510966757). J.S. gratefully acknowledges the financial support from the Carl Zeiss Foundation (Halocycles no. P2021-10-007). D.G. gratefully acknowledges funding from the Top Level Research Area SusInnoScience of the federal state of Rheinland-Pfalz. The authors thank Moritz Jahn and Tobias Rios-Studer for their helpful discussions.

Open Access funding enabled and organized by Projekt DEAL.

Conflict of Interest

The authors declare no conflict of interest.

Author Contributions

Dandan Gao: conceptualization (lead; funding acquisition (lead); project administration (lead); supervision (lead); writing—review & editing (lead); **Jennifer Christina Schmidt:** conceptualization (equal); writing—original draft (lead).

Keywords: 3D printing · electrocatalysis · electrochemical hydrodehalogenation · electrode design · trichloroacetic acid

[1] Z. Zhao, X. Yao, L. Zhang, R. Yu, Y. Xu, Y. Chu, X. Mao, H. Zheng, *EcoEnergy* **2024**, *2*, 83.
[2] R. Mao, N. Li, H. Lan, X. Zhao, H. Liu, J. Qu, M. Sun, *Environ. Sci. Technol.* **2016**, *50*, 3829.
[3] Y. Y. Lou, J. M. Fontmorin, A. Amrane, F. Fourcade, F. Geneste, *Electrochim. Acta* **2021**, *377*, 138039.
[4] M. Zhang, Q. Shi, X. Song, H. Wang, Z. Bian, *Environ. Sci. Pollut. Res.* **2019**, *26*, 10457.
[5] B. Huang, A. A. Isse, C. Durante, C. Wei, A. Gennaro, *Electrochim. Acta* **2012**, *70*, 50.
[6] G. Song, H. Wu, J. Jing, X. Zhang, X. Wang, S. Li, M. Zhou, *Environ. Sci. Technol.* **2023**, *57*, 14482.
[7] K. Yang, Y.-J. Kong, L.-Z. Huang, X.-M. Hu, *Chem. Eng. J.* **2022**, *450*, 138467.
[8] M. He, H. Wang, C. Cheng, R. Li, C. Liu, Y. Gao, B. Zhang, *J. Am. Chem. Soc.* **2025**, *147*, 5377.
[9] C. Liu, S. Han, M. Li, X. Chong, B. Zhang, C. Liu, S. Han, M. Li, X. Chong, B. Zhang, *Angew. Chem. Int. Ed.* **2020**, *132*, 18685.
[10] M. R. Flid, L. M. Kartashov, Y. A. Treger, *Catalysts* **2020**, *10*, 216.
[11] A. A. Isse, S. Gottardello, C. Durante, A. Gennaro, *Phys. Chem. Chem. Phys.* **2008**, *10*, 2409.
[12] H.-L. Lien, W.-X. Zhang, *Appl. Catal. B* **2007**, *77*, 110.
[13] X. Wang, C. Chen, Y. Chang, H. Liu, *J. Hazard. Mater.* **2009**, *161*, 815.
[14] Y. Guo, Y. Li, Z. Wang, *Water Res.* **2023**, *234*, 119810.
[15] L. Yang, Z. Chen, D. Cui, X. Luo, B. Liang, L. Yang, T. Liu, A. Wang, S. Luo, *Chem. Eng. J.* **2019**, *359*, 894.
[16] T. Liu, J. Luo, X. Meng, L. Yang, B. Liang, M. Liu, C. Liu, A. Wang, X. Liu, Y. Pei, J. Yuan, J. Crittenden, *J. Hazard. Mater.* **2018**, *358*, 294.
[17] L. Rajic, N. Fallahpour, E. Oguzie, A. Alshawabkeh, *Electrochim. Acta* **2015**, *181*, 118.
[18] J. V. Perales-Rondon, D. Rojas, W. Gao, M. Pumera, *ACS Sustainable Chem. Eng.* **2023**, *11*, 6923.
[19] J.-G. Mahy, T. Delbeuck, K.-Y. Tran, B. Heinrichs, S.-D. Lambert, *Gels* **2023**, *9*, 275.
[20] M. D. Esclapez, M. I. Díez-García, V. Sáez, I. Tudela, J. M. Pérez, J. González-García, P. Bonete, *Electrochimica Acta*, **2011**, *56*, 8138.
[21] H. Tang, Z. Bian, Y. Peng, S. Li, H. Wang, *J. Hazard. Mater.* **2022**, *433*, 128744.
[22] H. Yin, X. Cao, C. Lei, W. Chen, B. Huang, C. Reviews, *ChemElectroChem*. **2020**, *7*, 1825.
[23] A. A. Peverly, J. A. Karty, D. G. Peters, *J. Electroanal. Chem.* **2013**, *692*, 66.
[24] A. A. Rashid, W. Ahmed, M. Y. Khalid, M. Koç, *Addit. Manuf.* **2021**, *47*, 102279.
[25] A. K. K. Padinjareveetil, J. V. Perales-Rondon, M. Pumera, *Adv. Mater. Technol.* **2023**, *8*, 2202080.
[26] K. Rajan, K. K. Mahendran Samykano, W. Sharuzi, W. Harun, M. M. Rahman, *Int. J. Adv. Manuf. Tech.* **2022**, *120*, 1531.
[27] E. Bogdan, P. Michorczyk, *Materials* **2020**, *13*, 4534.
[28] H. Ramazani, A. Kami, *Prog. Addit Manuf.* **2022**, *7*, 609.
[29] K. Rajan, M. Samykano, K. Kadirgama, W. S. W. Harun, M. M. Rahman, *Int. J. Adv. Manuf. Technol.* **2022**, *120*, 1531.
[30] A. Lanzotti, M. Grasso, G. Staiano, M. Martorelli, *Rapid Prototyping J.* **2015**, *21*, 604.
[31] S. R. Rajpurohit, H. K. Dave, *Rapid Prototyp J.* **2018**, *24*, 1317.
[32] M. Taufik, P. K. Jain, *Aust. J. Mech. Eng.* **2020**, *20*, 527.
[33] M. A. S. R. Saadi, A. Maguire, N. T. Pottackal, M. S. H. Thakur, M. M. Ikram, A. J. Hart, P. M. Ajayan, M. M. Rahman, *Adv. Mater.* **2022**, *34*, 2108855.
[34] X. Wan, L. Luo, Y. Liu, J. Leng, *Adv. Sci.* **2020**, *7*, 2001000.
[35] Y. Zhang, W. Peng, Y. Cao, W. Wang, D. Teng, Y. Huang, G. Fan, *Colloids Surf. A Physicochem. Eng. Asp.* **2023**, *671*, 131603.
[36] C. E. Owens, R. J. Headrick, S. M. Williams, A. J. Fike, M. Pasquali, G. H. McKinley, A. J. Hart, *Adv. Funct. Mater.* **2021**, *31*, 2100245.
[37] A. Kessler, R. Hickel, M. Reymus, *Oper. Dent.* **2020**, *45*, 30.
[38] A. Fritschen, N. Lindner, S. Scholpp, P. Richthof, J. Dietz, P. Linke, Z. Guttenberg, A. Blaeser, *Adv. Healthc. Mater.* **2024**, *13*, e2304028.
[39] R. M. Cardoso, D. M. H. Mendonça, W. P. Silva, M. N. T. Silva, E. Nossol, R. A. B. da Silva, E. M. Richter, R. A. A. Muñoz, *Anal. Chim. Acta* **2018**, *1033*, 49.
[40] M. M. Garmabi, P. Shahi, J. Tjong, M. Sain, *Addit. Manuf.* **2022**, *56*, 102780.
[41] M. P. Browne, E. Redondo, M. Pumera, *Chem. Rev.* **2020**, *120*, 2783.
[42] D. P. Rocha, A. L. Squissato, S. M. da Silva, E. M. Richter, R. A. A. Munoz, *Electrochim. Acta* **2020**, *335*, 135688.
[43] J. Xu, P. Wang, S. Chen, L. Li, D. Li, Y. Zhang, Q. Wu, J. Fan, L. Ma, *J. Environ. Sci. (China)* **2024**, *137*, 420.
[44] Y. F. Zhang, J. L. Gao, S. G. Chen, L. Li, J. H. Xu, D. Li, Y. F. Liu, X. Quan, X. Fu, Y. Z. Xie, J. N. Wu, D. Y. Lin, T. T. Zheng, *Chem. Eng. J.* **2023**, *474*, 145561.
[45] H. Bulut, N. Demir, M. F. Kaya, *Fuel* **2024**, *366*, 131172.
[46] Y. Liu, J. Xu, X. Fu, P. Wang, D. Li, Y. Zhang, S. Chen, C. Zhang, P. Liu, *J. Environ. Sci.* **2024**, *135*, 108.
[47] L. Cao, J. Li, J. Hu, H. Liu, Y. Wu, Q. Zhou, *Opt. Laser Technol.* **2021**, *142*, 107246.
[48] J. Neukäufer, B. Seyfang, T. Grützner, *Ind. Eng. Chem. Res.* **2020**, *59*, 6761.
[49] R. A. Márquez, K. Kawashima, Y. J. Son, R. Rose, L. A. Smith, N. Miller, O. A. C. Jaim, H. Celio, C. B. Mullins, *ACS Appl. Mater. Interfaces* **2022**, *14*, 42153.
[50] T. Kou, S. Wang, R. Shi, T. Zhang, S. Chiovoloni, J. Q. Lu, W. Chen, M. A. Worsley, B. C. Wood, S. E. Baker, E. B. Duoss, R. Wu, C. Zhu, Y. Li, *Adv. Energy Mater.* **2020**, *10*, 2002955.
[51] R. Iwata, L. Zhang, K. L. Wilke, S. Gong, M. He, B. M. Gallant, E. N. Wang, *Joule* **2021**, *5*, 887.
[52] C.-Y. Lee, A. C. Taylor, S. Beirne, G. G. Wallace, *Adv. Energy Mater.* **2017**, *7*, 1701060.
[53] F. Yang, M. J. Kim, M. Brown, B. J. Wiley, *Adv. Energy Mater.* **2020**, *10*, 2001174.
[54] T. Chu, S. Park, K. Kun, K. Fu, *Carbon Energy* **2021**, *3*, 424.
[55] A. Limper, N. Weber, A. Brodersen, R. Keller, M. Wessling, J. Linkhorst, *Electrochem. commun.* **2022**, *134*, 107176.
[56] F. Wiesner, A. Limper, C. Marth, A. Brodersen, M. Wessling, J. Linkhorst, *Adv. Eng. Mater.* **2023**, *25*, 2200986.
[57] A. K. K. Padinjareveetil, M. Pumera, *Adv. Mater. Interfaces* **2023**, *10*, 2201734.
[58] B. Liu, H. Zhang, Q. Lu, G. Li, F. Zhang, *Sci. Total Environ.* **2018**, *635*, 1417.
[59] H. Mai, T. C. Le, D. Chen, D. A. Winkler, R. A. Caruso, *Chem. Rev.* **2022**, *122*, 13478.
[60] M. Asif, C. Yao, Z. Zuo, M. Bilal, H. Zeb, S. Lee, Z. Wang, T. Kim, *J. Ind. Eng. Chem.* **2025**, *144*, 32.
[61] X. Zhao, C. Karakaya, M. Qian, R. Zou, W. Zhang, Z. Lu, D. Maiti, A. Samanta, W. Wan, X. Liu, A. Tiplea, Y. Li, S. Cui, C. Wang, H. Lei, S. Bankston, S. Yilmaz, J. G. Chen, S. Ozcan, *Mater. Today Sustain.* **2024**, *26*, 100746.
[62] M. Javaid, A. Haleem, R. P. Singh, R. Suman, S. Rab, *Adv. Ind. Eng. Polym. Res.* **2021**, *4*, 312.
[63] J. J. Ong, B. M. Castro, S. Gaisford, P. Cabalar, A. W. Basit, G. Pérez, A. Goyanes, *Int. J. Pharm. X* **2022**, *4*, 100120.
[64] D. A. J. Brion, S. W. Pattinson, *Nat. Commun.* **2022**, *13*, 4654.
[65] T. Herzog, M. B. A. Trinchi, A. Sola, B. A. M. Molotnikov, *J. Intell. Manuf.* **2024**, *35*, 1407.
[66] L. Zhang, Q. Bing, H. Qin, L. Yu, H. Li, D. Deng, *Matter* **2025**, *8*, 102138.
[67] L. Zhu, Z. Lin, Y. H. Cui, S. K. Fang, Y. Wu, B. He, D. Liu, *Appl. Energy* **2026**, *403*, 127072.
[68] A. Prajapati, C. Hahn, I. M. Weidinger, Y. Shi, Y. Lee, A. N. Alexandrova, D. Thompson, S. R. Bare, S. Chen, S. Yan, N. Kornienko, *Nat. Commun.* **2025**, *16*, 2593.
[69] A. Prajapati, C. Hahn, I. M. Weidinger, Y. Shi, Y. Lee, A. N. Alexandrova, D. Thompson, S. R. Bare, S. Chen, S. Yan, N. Kornienko, *Nat. Commun.* **2025**, *16*, 2593.
[70] Z. Liu, N. Zhang, Y. Xiong, *J. Phys. Chem. C* **2024**, *128*, 13651.
[71] H. Liu, Z. Qi, L. Song, *J. Phys. Chem. C* **2021**, *125*, 24289.
[72] R. M. S. Yoo, D. Yesudoss, D. Johnson, A. Djire, *ACS Catal.* **2023**, *13*, 10570.
[73] R. Gao, J. Zhang, G. Fan, X. Wang, F. Ding, Y. Guo, C. Han, Y. Gao, A. Shen, J. Ding, L. Wu, X. Gu, *Angew. Chem., Int. Ed.* **2025**, *64*, e202505948.
[74] A. M. Abdellah, K. E. Salem, L.-A. DiCecco, F. Ismail, A. Rakhsha, K. Grandfield, D. Higgins, *Small Methods* **2025**, *9*, 2400851.
[75] J. Wang, C. S. Hsu, T. S. Wu, T. S. Chan, N. T. Suen, J. F. Lee, H. M. Chen, *Nat. Commun.* **2023**, *14*, 6576.

[76] O. M. Magnussen, J. Drnec, C. Qiu, I. Martens, J. J. Huang, R. Chattot, A. Singer, *Chem. Rev.* **2024**, *124*, 629.
[77] C. Griesser, S. Diaz-Coello, M. Olgiati, W. F. do Valle, T. Moser, A. Auer, E. Pastor, M. Valtiner, J. K. Liebhäuser, *Angew. Chem., Int. Ed.* **2025**, *64*, e202500965.
[78] N. R. Chodankar, S. J. Patil, S.-K. Hwang, P. A. Shinde, S. V. Karekar, G. S. Raju, K. S. Ranjith, A. G. Olabi, D. P. Dubal, Y.-S. Huh, Y.-K. Han, *Energy Storage Mater.* **2022**, *49*, 564.
[79] P. Oblak, J. Gonzalez-Gutierrez, B. Zupančič, A. Aulova, I. Emri, *Polym. Degrad. Stab.* **2015**, *114*, 133.
[80] F. A. C. Sanchez, H. Boudaoud, M. Camargo, J. M. Pearce, *J. Clean. Prod.* **2020**, *264*, 121602.
[81] L. F. Arenas, C. P. de León, F. C. Walsh, *Curr. Opin. Electrochem.* **2019**, *16*, 1.
[82] S. Stiefel, J. Lölsberg, L. Kipshagen, R. Möller-Gulland, M. Wessling, *Electrochem. Commun.* **2015**, *61*, 49.
[83] M. Lehmann, C. C. Scarborough, E. Godineau, C. Battilocchio, *Ind. Eng. Chem. Res.* **2020**, *59*, 7321.
[84] W. Xu, Z. Lu, X. Sun, L. Jiang, X. Duan, *Acc. Chem. Res.* **2018**, *51*, 1590.
[85] A. Angulo, P. van der Linde, H. Gardeniers, M. Modestino, D. F. Rivas, *Joule* **2020**, *4*, 555.
[86] D. Tilve-Martinez, P. Poulin, *Acc. Mater. Res.* **2025**, *6*, 661.
[87] A. C. Martinez, A. Maurel, A. P. Aranzola, S. Grugeon, S. Panier, L. Dupont, J. A. Hernandez-Viezcas, B. Mummareddy, B. L. Armstrong, P. Cortes, S. T. Sreenivasan, E. MacDonald, *Sci. Rep.* **2022**, *12*, 19010.
[88] L. Ladani, M. Sadeghilaridjani, *Metals (Basel)* **2021**, *11*, 1391.
[89] Z. Liu, Q. Zhou, X. Liang, X. Wang, G. Li, K. Vanmeensel, J. Xie, *Int. J. Extrem. Manuf.* **2024**, *6*, 022002.
[90] V. V. Popov, M. L. Grilli, A. Koptyug, L. Jaworska, A. Katz-Demyanetz, D. Klobčar, S. Balos, B. O. Postolnyi, S. Goel, *Materials* **2021**, *14*, 909.
[91] Z. Snow, R. Martukanitz, S. Joshi, *Addit. Manuf.* **2019**, *28*, 78.
[92] S. D. Jadhav, L. R. Goossens, Y. Kinds, B. Van Hooreweder, K. Vanmeensel, *Addit Manuf.* **2021**, *42*, 101990.
[93] A. Oleff, B. Küster, L. Overmeyer, *Int. J. Adv. Manuf. Technol.* **2022**, *123*, 1585.
[94] O. Gülcan, K. Günaydın, A. Tamer, *Polymers (Basel)* **2021**, *13*, 2829.
[95] E. Jabari, F. Liravi, E. Davoodi, L. Lin, E. Toyserkani, *Addit. Manuf.* **2020**, *35*, 101330.
[96] H. Miyanaji, D. Ma, M. A. Atwater, K. A. Darling, V. H. Hammond, C. B. Williams, *Addit. Manuf.* **2020**, *32*, 100960.
[97] S. Mirzababaei, S. Pasebani, *J. Manuf. Mater. Process* **2019**, *3*, 82.
[98] M. Ziaee, N. B. Crane, *Addit. Manuf.* **2019**, *28*, 781.
[99] N. K. Bankapalli, V. Gupta, P. Saxena, A. Bajpai, C. Lahoda, J. Polte, *Compos. Part B Eng.* **2023**, *264*, 110915.
[100] G. Wu, N. A. Langrana, R. Sadanji, S. Danforth, *Mater Des.* **2002**, *23*, 97.
[101] R. Arrigo, A. Frache, *Polymers (Basel)* **2022**, *14*, 1754.
[102] F. Cerejo, D. Gatões, M. T. Vieira, *Int. J. Adv. Manuf. Technol.* **2021**, *115*, 2449.
[103] Y. Li, B. S. Linke, H. Voet, B. Falk, R. Schmitt, M. Lam, *CIRP J. Manuf. Sci. Technol.* **2017**, *16*, 1.
[104] A. Kumar, A. R. Dixit, S. Sreenivasa, *Polym. Adv. Technol.* **2024**, *35*, e6396.
[105] K. T. Cho, L. Nunez, J. Shelton, F. Sciammarella, *J. Manuf. Mater. Process* **2023**, *7*, 105.

Manuscript received: October 15, 2025
Revised manuscript received: November 25, 2025
Version of record online: